JCBI
Journal of Computing & Biomedical Informatics Volume 10 Issue 02
ISSN: 2710 - 1606 2026

Research Article
https://doi.org/10.56979/1002/2026/1277

Reinforcement Squeeze-and-Excitation Learning for Automated Gleason Grading in Prostate Cancer Histopathology

Maulika Patel[1*], Parag Sanghani[1], and Niraj Shah[2]

[1]P P Savani University, Surat, Gujarat, India.
[2]School of Engineering, P P Savani University, Surat, Gujarat, India.
[*]Corresponding Author: Maulika Patel. Email: maulika.patel@ppsu.ac.in

Received: December 10, 2025 **Accepted:** February 27, 2026

Abstract: Proper diagnosis and treatment plans of prostate cancer can only be based on accurate Gleason grading of the prostate cancer using histopathological whole-slide images, and manual assessment is likely to be subject to inter-observer variability. This paper proposes a new Reinforcement Squeeze-and-Excitation Learning-based Convolutional Neural Network (RIL-SE-CNN) for automated Gleason grading. The framework combines reinforcement learning and squeeze-and-excitation blocks to dynamically recalibrate channel-wise features and enables focusing on diagnostically relevant glandular patterns. Reinforcement feedback is an optimal method for reinforcing the attention mechanism by rewarding discriminative feature representations across heterogeneous tissue regions. The proposed model is tested on two datasets, PANDA dataset and DiagSet-A dataset, using standard evaluation methods. On the PANDA dataset, the model achieved an accuracy of 96.46%, showing very good performance. On the DiagSet-A dataset, the model achieved a higher accuracy of 99.58%, which indicates that the model works very well on different datasets and gives strong and reliable results. These findings indicate the strength and generalization power of the proposed system for automated Gleason grading.

Keywords: Prostate Cancer Histopathology; Gleason Grading; Reinforcement Learning; Squeez-and-excitation Networks; Deep Learning

1. Introduction

Prostate cancer is a form of malignancy which has most frequently been diagnosed among men throughout the world and has remained a leading source of cancer morbidity and mortality. Histopathological examination of the prostate has taken the final diagnosis tool, and the Gleason grading system has taken the platform to assess the tumor aggressiveness and a foundation on which therapeutic decisions are made [1]. Despite its clinical impact, it is a subjective grading method, and its results are founded on the experience of the pathologists, which has resulted in inter- and interobserver variability particularly in tumors that have borderline and intermediate grades [2]. The solution to such limitations has been automated prostate cancer classification and grading, which are the topics of growing research on artificial intelligence (AI) and deep learning (DL) techniques. CNN models have demonstrated the potential of powerful discriminative morphological features in histopathological images, and ResNet-based models demonstrate superior feature extraction and classification accuracy [3]. Similar CNN techniques such as ProsGradNet extend to pay attention to architectural refinement in order to obtain glandular appearances [4], and parallel and multi-branch networks have been suggested to enhance multi-class discrimination in the task of prostate cancer grading [5].

Besides construction of innovations, other studies have also indicated that there is clinical imperative to employ reliable and reproducible grading systems. Diagnostic variability between biopsy techniques and pathological interpretation is also large and this influences clinical outcome [6]. Biochemical

recurrence and disease progression prediction methods have also been applied to the deep learning systems, where the prognostic value of appropriate Gleason grading is stressed [7]. Clinical studies on Gleason score upgrading [8] support the need to establish effective automated grading systems to lower diagnostic uncertainty. Recent trends have explored self-supervised learning to eliminate the need of annotations [9] and vision transformer-driven designs to learn long-range spatial features in histopathological images [10]. pre-defined datasets like DiagSet have made it possible to perform standard benchmarking of prostate cancer classification methods [11]. Furthermore, secondary workflows with AI support and trained deep belief networks are optimized [12], and AI-based developments in the pathology field are proved to be translatable in clinical practice [13].

It has been suggested that multi-scale and patch-level learning can be applied to the problem of working with whole-slide images and provide a powerful computational treatment of the high-resolution histopathology data [14]. The comparative studies of deep learning models show that, despite the possibility of high accuracy, there are deficiencies in generalization, robustness, and interpretability of the deep learning models on different datasets [15]. The variation of the labels, and the absence of classes have contributed to the implementation of the ensemble-based learning methods to minimize the variability of grading [16]. There has also been exploration of lightweight and computationally effective architectures to be useful [17], and techniques such as selective CutMix to augment data to improve model generalization [18]. Transformer-based gland segmentation structures are also used to enhance grading by enhancing the localization of features at the level of a region [19]. The clinical value of proper grading is emphasized by machine learning techniques of predicting the Gleason improvement between biopsy and prostatectomy samples [20]. The federated learning paradigms have been designed to provide the possibility of simultaneous model training without data privacy loss [21] and AI creation in its general use in prostate cancer management [22].

Despite such developments, these are, however, some of the key gaps. The available models are mostly of a classical approach in which the mechanisms of attention do not meet the dynamic requirement of heterogeneous forms of glands and tissue. Recent articles emphasize the need of interpretable AI systems that can produce clinically significant explanations [23], but systematic reviews present unexplored problems with robustness, flexibility, and clinical trust [24] and [25]. The existing evaluation research yields evidence that the performance declines when models apply between institutions and data sets [26], and comparative research evidence indicates that there are never no differences between AI-based grading and human pathologists [27]. Other techniques, including label distribution learning [28] or radiomics-based grading [29], supply complementary data but are not adequate to explain complicated histopathological variations. The necessity of adaptive feature-emphasis processes is also confirmed by the gland-level malignancy classification [30] and the recent biomarkers of histopathology [31]. It has been conclusively demonstrated that attention-sensitive scaleable deep learning systems are necessary to provide robust automated Gleason grading [32]. These limitations have motivated this work and introduced a CNN with reinforcement squeeze-and-excitation learning (RIL-SE-CNN) that uses reinforcement learning to dynamically optimize channel-wise feature recalibration. The objectives are to enhance accuracy of grading, generalization of grading between datasets, and reducing grading ambiguity. The remainder of this paper will follow the following format: The literature review section II, Proposed materials and methods section III, Section IV will be the experimental findings and analysis, and Section V will be the conclusion of the research and future research directions.

2. Related Works

The past few years have been marked by faster development of artificial intelligence to analyze the histopathology of prostate cancer and most of it is related to automate Gleason grading. The earliest deep learning models employed convolutional neural networks (CNNs) as their main hierarchical feature extractor in the histopathology image. ResNet models also performed more classification accuracy due to the minimization of the vanishing gradient issue and the ability to learn more features [1]. They also enhanced discriminative performance with hybrid deep learning models that used CNNs in conjunction with handcrafted or optimized feature representations, particularly on complex tissue patterns [2]. It was suggested that task-inspired architectural designs, such as ProsGradNet, could be used as structured CNN models that enhanced the stability of glandular morphology, thus offering more grading consistency [3].

Similarly, multichannel and contribution-aware networks concerned with learning complementary channel properties, and the importance of attention-like processes to prostate cancer grading was noted [4]. Parallel branch networks were also suggested to address the multi-class classification issue and led to large gains with regard to the grading accuracy [5].

Besides architectural design, other studies have investigated the clinical implication of correct Gleason grading. It is also revealed that the difference in diagnosis of the biopsy strategies and pathological interpretation can significantly influence the treatment outcomes [6]. Deep learning systems are aimed at predicting biochemical recurrence, which underlies prognostic characteristics of histopathological grading [7]. The investigations of Gleason score upgrading performed by the clinic provide additional evidence of the necessity of the creation of effective automated grading systems reducing diagnostic uncertainties [8]. All these facts drive home the point that any computation model must not only be accurate but also robust and clinically relevant.

Transformer-based and self-supervised learning paradigms have been presented to tackle the problem of the limited availability of annotations and improve generalization of features. Unlabeled data is used in self-supervised grading techniques which find meaningful representations without a large number of annotations [9]. The reason has been the use of vision transformers since they are capable of capturing long-range spatial dependencies in histological images, an alternative to models that do not rely on CNN. It has been demonstrated that with the release of curated datasets such as DiagSet [11], standardized evaluation and benchmarking of prostate cancer classification models are now possible. Second, optimized deep belief networks have also been effective in Gleason grading tasks [12], and AI-assisted second-read systems have also been demonstrated to be potentially applicable in the real world [13].

Whole-slide images contain very high-resolution images, which are spatially inhomogeneous, making their analysis computationally challenging. This has been highly adopted using multi-scale and patch-level learning strategies [14]. Comparative analysis of the deep learning approaches demonstrates that the high-performance results may be obtained in case of controlled conditions, though inter-dataset generalization is a severe problem [15]. The distortions in labels and scoring disparity have supported the use of the ensemble learning techniques to facilitate resilience [16]. To attain quicker inference and clinical feasibility, lightweight and efficient deep learning models have been suggested as well [17]. It has been shown that the generalization and overfitting [18] of data augmentation methods, such as selective CutMix, are positive. Transformer-based gland segmentation schemes are also useful in grading because they increase the localization of regions [19].

More recent studies have generalized automated grading to the predictive and federated learning models. The machine learning models of Gleason grade prediction trained on biopsy and prostatectomy samples are useful in decision support [20]. Federated learning techniques allow institutions to collaboratively train one model and maintain the privacy of data, which is a significant barrier to massive clinical adoption [21]. Longer articles dwell on the radical role of AI in treating prostate cancer and mention the need to explain and have clinical trust [22], [23]. Large-scale surveys have both discovered that AI-based Gleason grading systems still suffer interpretability, robustness, and bias in datasets problems [24], [25]. In performance degradation, external validation experiments reveal that models cannot be used optimally in a heterogeneous clinical environment [26], and comparative studies indicate that AI predictions and expert pathologists have considerable differences [27].

Alternative approaches to learning which include label distribution learning [28] and Gleason score prediction using radiomics [29] are other learning paradigms that fail to resolve subtle histopathological variability. The gland-level malignancy classification techniques are characterized by paying a particular focus to the local features [30], and novel feature biomarkers are to remind the necessity of adaptive and discriminative features learning [31]. PANDA challenge has clearly shown that attention-based deep learning models are a key to the scalable, reliable automated Gleason grading [32].

According to the literature reviewed, although deep learning models are highly accurate in their grading, most currently existing methods apply a constant attention or fixed feature weighting scheme. These limitations reduce flexibility to non-homogeneous tissue patterns and play a role in reduced extrapolation to datasets. In addition, we also do not lack a research gap with respect to the insufficient combination of reinforcement-based optimization and dynamic feature recalibration. Such results confirm

the suggested Reinforcement Squeeze-and-Excitation Learning model that dynamically regulates channel focus on features to encourage strong and reliable Gleason grading.

3. Proposed Work

This part presents the suggested Reinforcement Squeeze-and-Excitation Convolutional Neural Network (RIL-SE-CNN) model of automated Gleason grading of prostate cancer histology. **Figure 1** illustrates the overall architecture and learning process and indicates how convolutional feature extraction, squeeze-and-excitation (SE)-based channel recalibration and reinforcement learning-based optimization are combined. The suggested system will optimize the discriminative feature representations dynamically to improve the grading accuracy and robustness on heterogeneous histopathological patterns by feedback on the reinforcement learning.

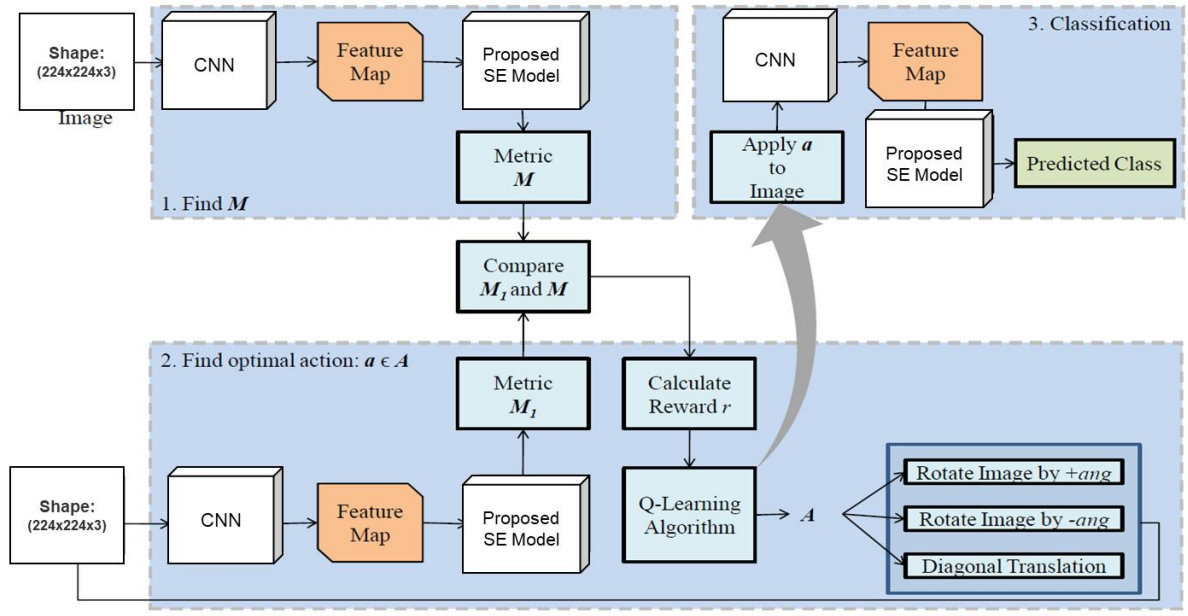

Figure 1. Novel RIL-SE-CNN System Framework

Pseudo Code:

Step 1: Load dataset $(\boldsymbol{I}, \boldsymbol{y})$
Step 2: Preprocessing
Resize $I \rightarrow 224 \times 224 \times 3$
Normalize image
Step 3: Feature Extraction (CNN)
Extract feature representation from I
Step 4: SE Model & Metric Computation
Apply SE model
Compute metric M
Define state $s = (\text{feature}, M)$
Step 5: Q-Learning (Action Selection & Transformation)
Select action $a \in A$using $Q(s, a)$
Apply transformation $\rightarrow I'$
Step 6: Update Metric (After Action)
Pass I' through CNN-SE
Compute updated metric M_1
Compute reward: $r = M_1 - M$
Update Q-table: $Q(s_t, a_t) \leftarrow Q(s_t, a_t) + \alpha[r_t + \gamma \max_{a'} Q(s_{t+1}, a') - Q(s_t, a_t)]$
Step 7: Model Classification
Use transformed image I'
Predict class using SE-CNN

Step 8: Model Update
Update SE-CNN learning parameters
Step 9: Policy

$$\pi^*(s) = \arg\max_a Q(s, a)$$

Step 10: Repeat process until 50 epochs

3.1. Input Data and Preprocessing.

The suggested framework works on the RGB histopathological image patches 224 x 224 x 3, which have been cut out of the whole-slide images (WSIs). Before training models, standard preprocessing measures are performed to normalize variations in staining and enhance stability in learning. The steps that are involved are recalibration of the size, normalization of pixel intensity, and augmenting of the data. To enhance model generalization, augmentation operations, which include rotation, diagonal translation and controlled angular transformations, are further added to the reinforcement learning stage. The normalization of the input shape makes it compatible with CNN backbone and enables batch processing with ease.

3.2. CNN-Based Feature Extraction

The first step in the RIL-SE-CNN architecture is to use a convolutional neural network to identify high-level spatial and semantic features in the input histopathological images, as illustrated in **Figure 2**. The CNN backbone consists of several convolutional layers, nonlinear activation functions, and pooling layers. These layers increasingly represent low-level texture data, glandular morphology, and other higher-order structural patterns that are important to Gleason grading.

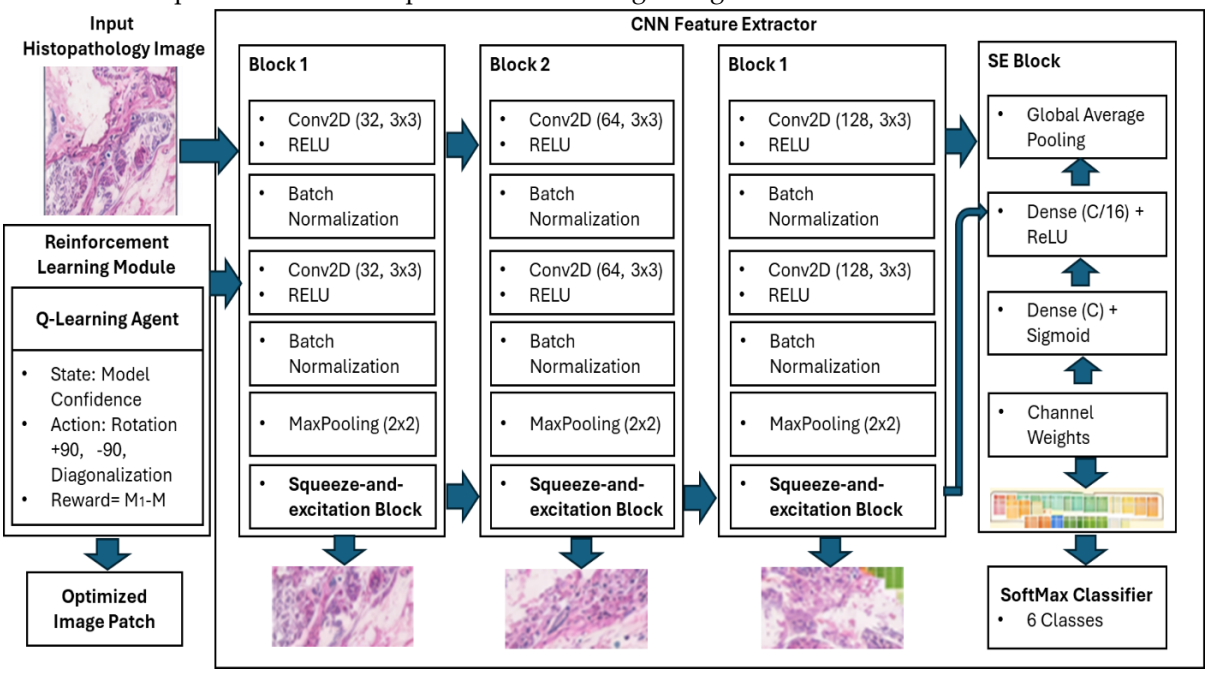

Figure 2. Custom CNN Backbone Architecture

The CNN output is a feature map, which serves as the input to the proposed squeeze-and-excitation (SE) module. In this feature map, spatially distributed representations that capture differences in gland shape, lumen structure, and epithelial organization, which are important cues in identifying Gleason patterns, are encoded.

3.3. Squeeze-and-Excitation (SE) Model Proposal

The suggested SE model is instrumental in feature recalibration in a channel-wise manner. In contrast to traditional SE blocks, which use fixed attention weights, the proposed solution deploys adaptive feature recalibration with the assistance of reinforcement learning. SE model has three key operations which include squeeze, excitation and feature scaling.

The squeeze phase makes use of global average pooling in CNN feature map to produce a channel-wise depiction that encodes the global contextual data. It is a descriptive statistic that indicates the value

of every feature channel in the spatial dimensions. During the excitation stage, the descriptor is run through a series of fully connected layers using nonlinear activation functions to produce weights of channel importance. These weights are the weight of each channel of Gleason grading. Last, during the feature scaling stage, the original feature map is scaled by multiplying it by the learned channel weights which prioritizes the diagnostically meaningful features and emphasizes the redundant or noisy channels.

3.4. Computation and State Definition

Metric Computation Metric computation involves performing arithmetic operations on numbers expressed in units of a standard-length measurement (measurand), typically the meter or foot. Figure 1 above shows that a performance measurement M, which serves as the baseline state in the reinforcement process learning, is computed using the recalibrated feature map, as shown in Step 1 (Find M). The measure can be expressed as classification confidence, loss value, or feature discrimination quality based on the SE-enhanced representation. This measure summarizes the system's prevailing condition prior to reinforcement-based optimization. Next, the system examines other transformations by performing actions on the input image, resulting in a new metric M_1. The difference between M and M_1 provides a quantitative measure of improvement or degradation resulting from the chosen action.

Measurement M in the reinforcement learning model corresponds to the confidence of the CNN-SE model for a particular histopathological image patch used in Gleason grading. The SoftMax classifier yields probability scores for the six Gleason grades after both the CNN feature extractor and the squeeze-and-excitation module process the image. M is a metric used to define the most likely prediction for these classes, and it shows the model's confidence in its Gleason grade predictions.

3.5. Reinforcement Learning Formulation

The reinforcement learning sub-unit will focus on the dynamic regulation of features and data transformation recalibration. The CNN-SE model pipeline determines the learning environment, and it is the responsibility of the agent to select the most appropriate actions to maximize performance during grading.

1) State Space

The feature representations that have been extracted and the performance measure (M or M_1) characterize the state. This formulation allows the agent to determine how the focus on the features and data transformations influences the classification performance.

2) Action Space

The action space A contains a set of pre-defined image operations, which are:

- Image rotation of a positive angle, +ang,
- Anticlockwise rotation of the image (-ang),
- The picture is diagonally shifted.

The choices are taken to amplify invariance to spatial orientation and morphological variability in histopathological slides that are frequently met.

3) Reward Function

Reward r is based on the comparison of M and M_1 as illustrated in the structure. Where the desired action leads to desirable change in the measure of performance, there is a positive reward given, whereas where undesirable change in the performance measure is realized, a negative reward or no reward is given. Such reward scheme motivates the agent to devise transformation strategies to promote the discrimination of features and the guaranteeing classification.

3.6. Q-Learning Optimization

The reinforcement learning agent uses a Q-learning algorithm to find out the best action policy.

$$Q(s_t, a_t) \leftarrow Q(s_t, a_t) + \alpha[r_t + \gamma \max_{a'} Q(s_{t+1}, a') - Q(s_t, a_t)] \quad (1)$$

Where s_t= state (feature vector + metric M), a_t= selected transformation, r_t= reward ($M_1 - M$), α= learning rate, and γ= discount factor.

Define policy:

$$\pi^*(s) = \arg\max_a Q(s, a) \quad (2)$$

The Q-learning module updates the action-value function based on the reward received and the expected future rewards. The agent learns an optimal policy through trial-and-error interactions with the environment, and it can choose the best transformation to apply to a particular state. The input image is then fed to the learned action policy A as shown by the Feedback loop in **Figure 1**. This adaptive mechanism allows the model to sharpen feature representations as training proceeds, resulting in enhanced resistance to intra- and staining variation. The state passed to Q-learning consists of a 100,352-dimensional CNN feature vector along with a 6-dimensional SoftMax probability vector representing Gleason grade confidence.

3.7. Classification Stage

The last step is Classification, during which the optimized action policy is applied to the input image. The CNN and the proposed SE model are applied to the transformed image to produce an improved feature map. This feature map is then passed to a classification head composed of fully connected layers and a SoftMax activation function. The network produces a Gleason class estimate based on the input image.

3.8. Training Strategy and Implementation Details

The RIL-SE-CNN framework is end-to-end trained by combining supervised classification loss with reinforcement-based optimization. The CNN and SE parameters are trained by backpropagation, and the action-value function is trained separately by the reinforcement learning module. The hybrid learning approach can optimize feature extraction, attention recalibration, and transformation selection simultaneously. Patches extracted using tumor-mask guided sampling. Only patches with >70% tumor tissue retained. Background patches excluded. If random sampling is used, state stratified random sampling.

3.9. Benefits of the Proposed Framework

The proposed RIL-SE-CNN model has several benefits:

- Reinforcement learning-based dynamic channel-wise feature recalibration,
- Greater generalization with adaptive image transformations,
- Large-scale management of histopathological heterogeneity and increased differentiation of near Gleason patterns.

In general, the suggested methodology is a unified and adaptive approach toward automated Gleason grading which successfully combines the principles of deep learning and reinforcement learning to reach high diagnostic performance.

4. Results

The proposed RIL-SE-CNN model was deployed and tested on a Kaggle cloud-based execution platform to ensure reproducibility and efficient computation. The network was supplied with histopathological image patches of size 224 × 224 × 3 as inputs and was configured to predict six ISUP grade groups (0-5) based on the severity of prostate cancer. The experiments were trained for 50 epochs with the Adam optimizer, an initial learning rate of 0.001, and a batch size of 64. Two publicly available datasets, including the PANDA dataset retrieved from the Kaggle repository xhlulu/panda-resized-train-data-512x512 and the DiagSet-A dataset retrieved from the official GitHub repository michalkoziarski/DiagSet, were used to train and validate the model. A 5-fold cross-validation strategy was used to guarantee sound and impartial performance assessment. To guarantee the reliability of performance evaluation and prevent overfitting, a 5-fold cross-validation approach was adopted. The sample was stratified into more than five mutually exclusive subsets of equal size, and the classes were sampled randomly to maintain the same proportions. The standard classification metrics used to measure model performance would include:

Accuracy (ACC): Refers to the overall percentage of images of histopathology correctly classified with all predictions on ISUP grade.

$$\text{ACC} = \frac{TP+TN}{TP+TN+FP+FN} \quad (3)$$

Precision (P): Refers to the number of images, which are correctly predicted to be of a particular ISUP grade, which is a measure of prediction reliability.

$$\text{Precision} = \frac{TP}{TP+FP} \quad (4)$$

Recall (R): Tests the model to understand its capability to correctly recognize histopathology images of a specific grade of ISUP.

$$\text{Recall} = \frac{TP}{TP+FN} \quad (5)$$

F1-Score: It is a harmonic average between precision and recall and it balances between false positives and false negatives of the ISUP grade classification.

$$\text{F1-Score} = \frac{2\times\text{Precision}\times\text{Recall}}{\text{Precision}+\text{Recall}} \quad (6)$$

Matthews Correlation Coefficient (MCC): The balanced measure of performance, which takes into account all the elements of confusion matrices, especially useful in multi-class and imbalanced ISUP grading.

$$\text{MCC} = \frac{(TP\times TN)-(FP\times FN)}{\sqrt{(TP+FP)(TP+FN)(TN+FP)(TN+FN)}} \quad (7)$$

4.1. PANDA Dataset

Figure 3 illustrates sample histopathological images of the given ISUP grades (0 to 5), where 800 images are assigned to each of them. The pictures illustrate the various stages of prostate cancer severity, from benign (grade 0) to most aggressive (grade 5), showing the visual differences the model is expected to differentiate.

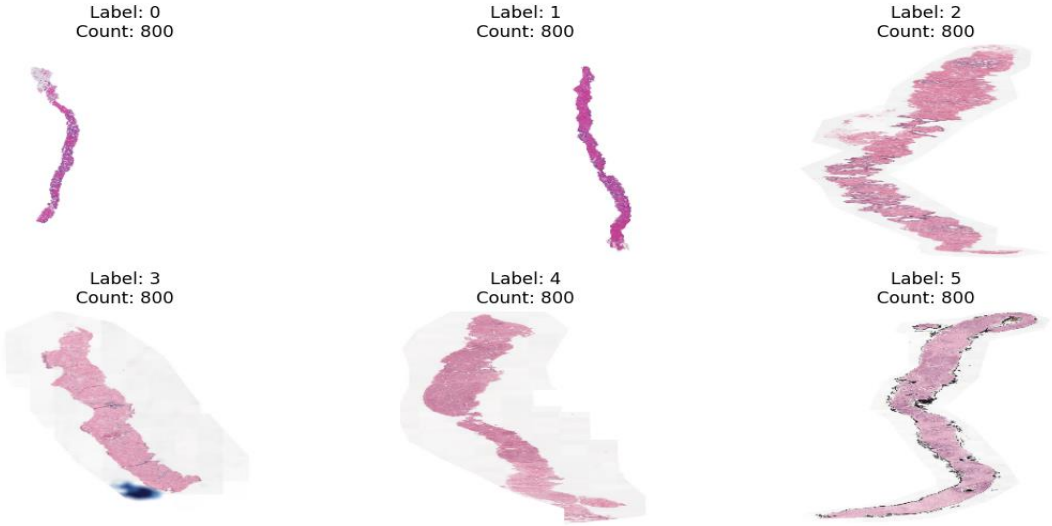

Figure 3. PANDA Dataset Reading

The training and validation accuracies (left) and losses (right) over 50 epochs are shown in Figure 4. The training accuracy converges quickly to 1.0, whereas the validation accuracy fluctuates. Validation loss is less stable than training loss, so it may be overfit at the beginning of training.

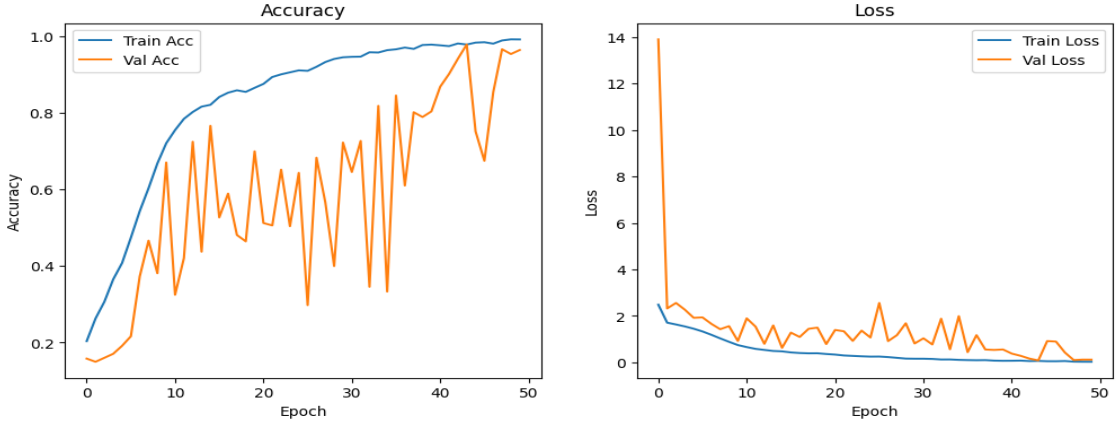

Figure 4. Accuracy and Loss Plot

Figure 5 indicates the confusion table of the six ISUP grades (0 5). There are several model-wise predictions that align along the diagonal, and the model is very good overall. The major misclassifications are those that happen between adjacent grades, especially the grades 2 and 3.

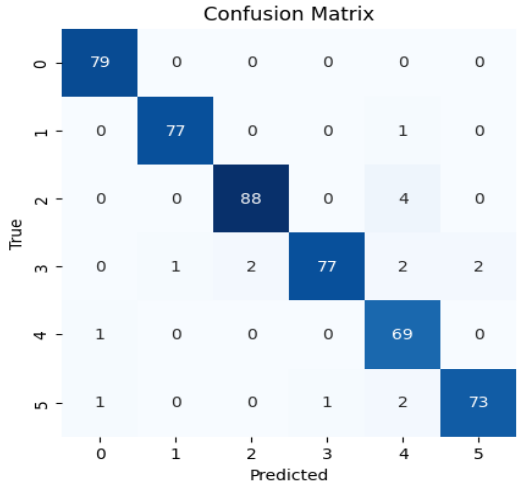

Figure 5. Confusion Matrix

As shown in Figure 6, classification report the proposed model accuracy on PANDA dataset is 96.46%. Grades 1 to 3 precision score high in all measurements. Grade 4 is less precise 88.46%, which implies that there would be some false positives.

Classification Report:

	precision	recall	f1-score	support
0	0.9753	1.0000	0.9875	79
1	0.9872	0.9872	0.9872	78
2	0.9778	0.9565	0.9670	92
3	0.9872	0.9167	0.9506	84
4	0.8846	0.9857	0.9324	70
5	0.9733	0.9481	0.9605	77
accuracy			0.9646	480
macro avg	0.9642	0.9657	0.9642	480
weighted avg	0.9662	0.9646	0.9647	480

Figure 6. Classification Report

Figure 7 demonstrates the 5-fold cross validation of the given RIL-SE-CNN model, which reported similar results in all folds, which indicates the stability and reliability of the proposed framework.

	Fold	Accuracy	Precision	Recall	F1-Score	MCC
0	1	0.9688	0.9704	0.9688	0.9688	0.9628
1	2	0.9677	0.9689	0.9677	0.9677	0.9615
2	3	0.9750	0.9762	0.9750	0.9751	0.9702
3	4	0.9646	0.9657	0.9646	0.9647	0.9577
4	5	0.9708	0.9716	0.9708	0.9709	0.9651

Average Scores:

Fold	3.00000
Accuracy	0.96938
Precision	0.97056
Recall	0.96938
F1-Score	0.96944
MCC	0.96346

Figure 7. K-Fold Validation

4.2. DiagSet-A Dataset

Sample histopathological images (n=800) of each grade of ISUP (0 to 5) are presented in Figure 8. The pictures are an illustration of the various stages of the severity of prostate cancers, i.e., benign (grade 0) to most aggressive (grade 5), illustrating the visual differences that the model is expected to differentiate.

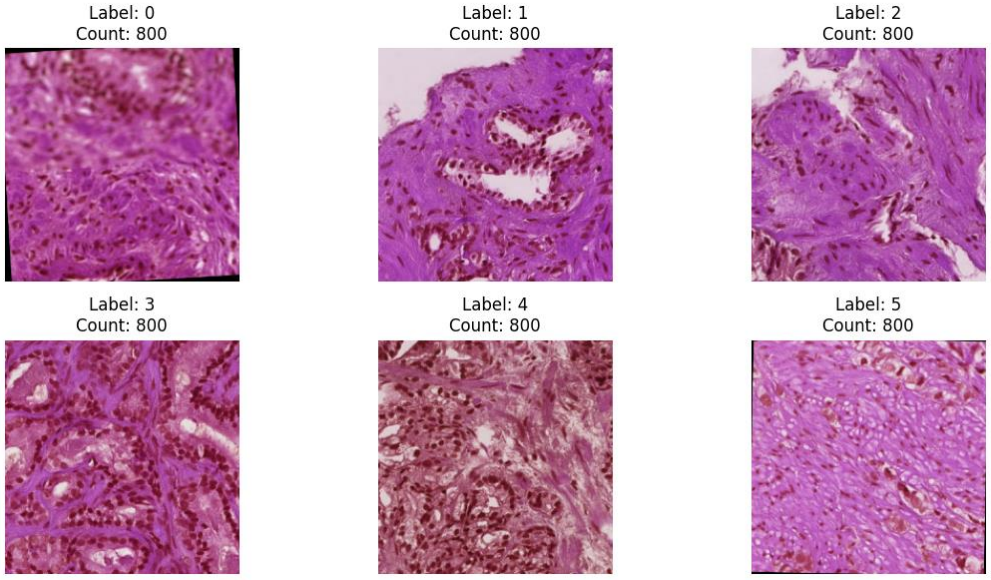

Figure 8. DiagSet-A Dataset Reading

Figure 9 shows the training and validation accuracy (left) and loss (right) quantities for 50 epochs. The accuracy of training fast converges to 1.0, whereas the validation accuracy increases with additional fluctuation. Validation loss is not as stable as the training loss, so it may overfit at the beginning of training.

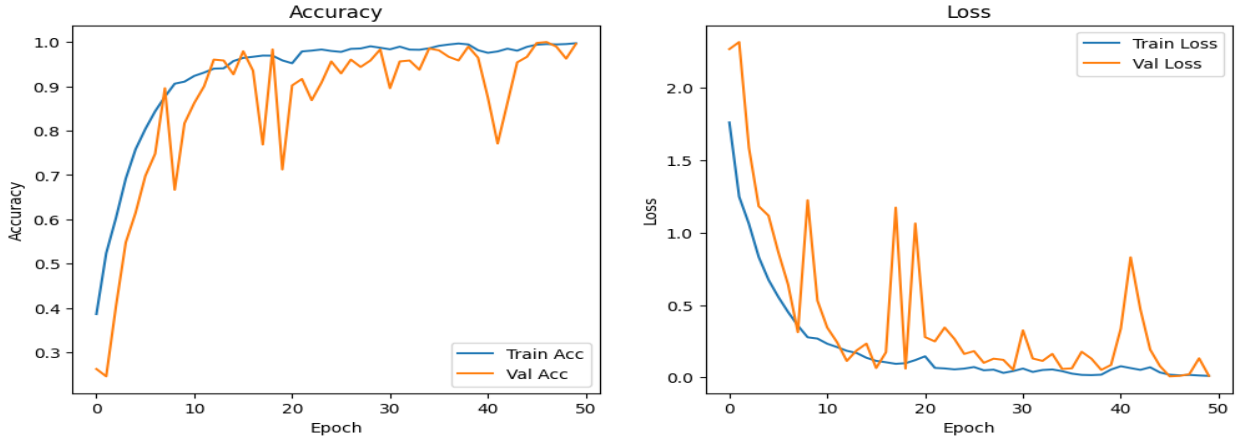

Figure 9. Accuracy and Loss Plot

The confusion matrix of the six grades of ISUP is presented in Figure 10. There are several model-wise predictions that align along the diagonal, and the model is very good overall. The major misclassifications are those that happen between adjacent grades, especially the grades 2 and 3.

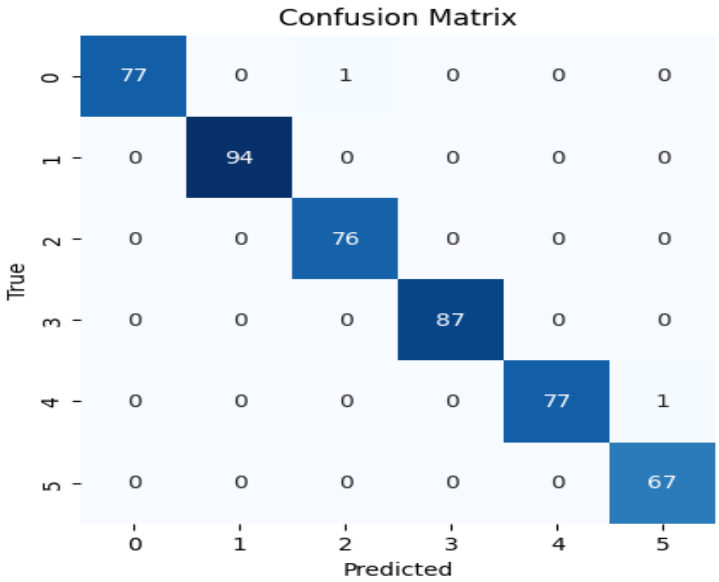

Figure 10. Confusion Matrix

As shown in **Figure 11**, classification report the proposed model accuracy on Diagset-A dataset is 99.58%. Grades 0, 1, 3 and 4 precision score high in all measurements.

Classification Report:

	precision	recall	f1-score	support
0	1.0000	0.9872	0.9935	78
1	1.0000	1.0000	1.0000	94
2	0.9870	1.0000	0.9935	76
3	1.0000	1.0000	1.0000	87
4	1.0000	0.9872	0.9935	78
5	0.9853	1.0000	0.9926	67
accuracy			0.9958	480
macro avg	0.9954	0.9957	0.9955	480
weighted avg	0.9959	0.9958	0.9958	480

Figure 11. Classification Report

Figure 12 demonstrates the 5-fold cross validation of the given RIL-SE-CNN model, which reported similar results in all folds, which indicates the stability and reliability of the proposed framework.

	Fold	Accuracy	Precision	Recall	F1-Score	MCC
0	1	0.9969	0.9969	0.9969	0.9969	0.9963
1	2	0.9979	0.9979	0.9979	0.9979	0.9975
2	3	0.9990	0.9990	0.9990	0.9990	0.9988
3	4	0.9969	0.9969	0.9969	0.9969	0.9963
4	5	0.9948	0.9949	0.9948	0.9948	0.9938

Average Scores:

Fold	3.00000
Accuracy	0.99710
Precision	0.99712
Recall	0.99710
F1-Score	0.99710
MCC	0.99654

Figure 12. K-Fold Validation

The convergence behavior of the Q-learning agent during training was considered to assess the stability of the reinforcement learning component. The agent continuously improves the action-value function using the reward of action by transforming the image. The reward is determined as the difference of model confidence of the original and transformed image: and M is the classification confidence of the existing state and M_1 is the confidence after the transformation that is selected has been applied.

$$r = M_1 - M \tag{8}$$

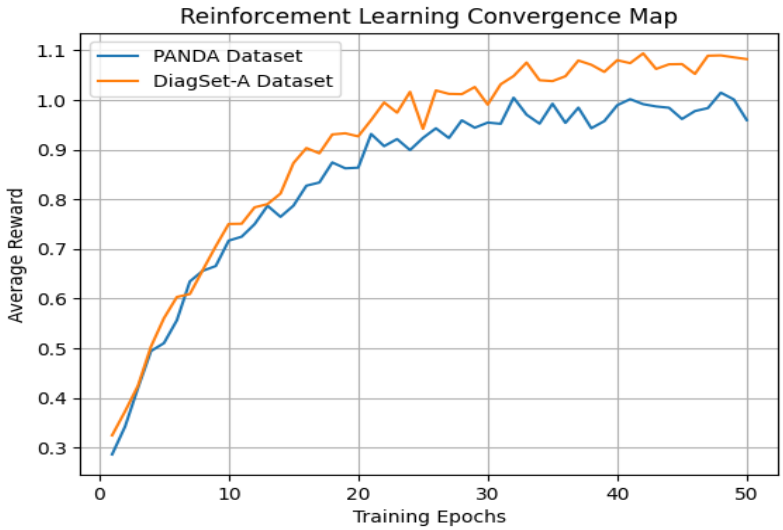

Figure 13. Convergence Map

The convergence map in the reinforcement learning process is shown in **Figure 13.** The result of the plot demonstrates the average cumulative reward that the Q-learning agent achieves in training episodes. The reward becomes constant with increasing the number of episodes, which means that the agent manages to learn an optimal policy to choose the most effective image transformations. Such convergence proves the efficiency of the reinforcement learning in controlling the adaptive feature focus in the proposed RIL-SE-CNN framework.

5. Discussion

Table 1 illustrates a comparison of performance between current models of deep learning and a newly proposed RIL-SE-CNN framework on DiagSets-A and PANDA. The proposed method demonstrates high accuracy, F1-score, and MCC and is significantly better than the traditional CNN, transformer, and ensemble-based methods, which makes it more robust and has a high generalization ability in automated Gleason grading.

Table 1. Comparative Analysis

Model	Dataset	ACC	Precision	Recall	F1-Score	MCC
ResNet-50 [2]	PANDA	89.00%	89.00%	88.00%	89.00%	-
Self-Supervised ViT [4]	PANDA	89.00%	87.00%	88.00%	89.00%	-
Optimized Deep Belief Network (DBN) [6]	PANDA	87.00%	89.00%	85.00%	87.00%	-
Multi-Label Ensemble CNN [10]	PANDA	89.00%	91.00%	88.00%	89.00%	-
Efficient CNN [11]	PANDA	88.00%	90.00%	87.00%	88.00%	-
SE-CNN	PANDA	94.00%	95.00%	94.00%	94.00%	94.00%
Proposed RIL-SE-CNN	PANDA	96.46%	96.42%	96.57%	96.42%	96.34%
Proposed RIL-SE-CNN	DiagSet-A	99.58%	99.54%	99.57%	99.55%	99.65%

6. Conclusions

The research presented a new Convolutional Neural Network (RIL-SE-CNN) based on Reinforcement Squeeze-and-Excitation Learning, which can be applied to automated Gleason grading of prostate cancer histopathology. By combining reinforcement learning with squeeze-and-excitation processes, the proposed framework adapts channel-specific feature relevance in real time, enabling adaptive stress on diagnostically significant glandular patterns and the suppression of redundant information. The optimization with reinforcement also enhances robustness by acquiring effective transformation strategies

during training. The proposed model is tested on two datasets, PANDA dataset and DiagSet-A dataset, using standard evaluation methods. On the PANDA dataset, the model achieved an accuracy of 96.46%, showing very good performance. On the DiagSet-A dataset, the model achieved a higher accuracy of 99.58%, which indicates that the model works very well on different datasets and gives strong and reliable results.

The proposed solution is a valid scalable automated system of prostate cancer grading with high potential of application in clinical decision-support systems. The future work will also aim at extending multi-instance learning, enhancing interpretability with attention visualization, and validation in the significantly larger cohort of multi-institutions to allow further clinical applications.

Supplementary Materials: Not Applicable.
Funding: Not Applicable.
Data Availability Statement: Not Applicable.
Acknowledgments: Not Applicable.
Conflicts of Interest: The authors declare no conflict of interest.

References

1. Emegano, D.I., Mustapha, M.T., Ozsahin, D.U., Ozsahin, I., Uzun, B.: Histopathology-Based Prostate Cancer Classification Using ResNet: A Comprehensive Deep Learning Analysis. Journal of Imaging Informatics in Medicine. (2025). https://doi.org/10.1007/s10278-025-01543-1.
2. Poonkuzhali, P., Krishnamoorthy, R., Nimma, D., Ramesh, J.V.N.: Prostate cancer prediction through a hybrid deep learning method applied to histopathological image. Expert Review of Anticancer Therapy. (2025). https://doi.org/10.1080/14737140.2025.2512040.
3. Prabhu, A., Nedungatt, S., Lal, S., Kini, J.: ProsGradNet: An effective and structured CNN approach for prostate cancer grading from histopathology images. Biomedical Signal Processing and Control. 105, 107626 (2025). https://doi.org/10.1016/j.bspc.2025.107626.
4. Qiu, J., Chen, Q., Lan, W., Cao, J.: Multichannel Contribution Aware Network for Prostate Cancer Grading in Histopathology Images. Journal of Computational Biology. (2025). https://doi.org/10.1089/cmb.2024.0872.
5. Srivastava, V., Prabhu, A., Nedungatt, S., Vibha Damodara, K., Lal, S., Kini, J.: An Efficient Parallel Branch Network for Multi-Class Classification of Prostate Cancer From Histopathological Images. International Journal of Imaging Systems and Technology. 35, e70092 (2025). https://doi.org/10.1002/ima.70092.
6. Kania, E., Janica, M., Hrehoruk, G., Kurowski, P., Ostasiewicz, A., Samocik, P., Kozłowski, R., Janica, J.R.: Enhancing Prostate Cancer Diagnosis: A Comparative Analysis of Combined Fusion and Systematic Biopsy Methods—A Single-Center Study. Journal of Clinical Medicine. 14, 2822 (2025). https://doi.org/10.3390/jcm14082822.
7. Cao, L., He, R., Zhang, A., Li, L., Cao, W., Liu, N., Zhang, P.: Development of a deep learning system for predicting biochemical recurrence in prostate cancer. BMC Cancer. 25, (2025). https://doi.org/10.1186/s12885-025-13628-9.
8. Esen, B., Gürses, B., Özkan, A., Kiliç, M., Kordan, Y., Esen, T., Ertoy Baydar, D.: Predictors of gleason score upgrading in patients with a biopsy diagnosis of grade group 1 prostate cancer. Turkish Journal of Medical Sciences. 55, 231–236 (2025). https://doi.org/10.55730/1300-0144.5962.
9. Bhattacharyya, R., Das, S.P., Mitra, S.: Efficient Self-Supervised Grading of Prostate Cancer Pathology. arXiv. (2025).
10. Chaurasia, A.K., Harris, H.C., Toohey, P.W., Hewitt, A.W.: A generalised vision transformer-based self-supervised model for diagnosing and grading prostate cancer using histological images. Prostate Cancer and Prostatic Diseases. 1–9 (2025). https://doi.org/10.1038/s41391-025-00957-w.
11. Koziarski, M., Cyganek, B., Niedziela, P., Olborski, B., Antosz, Z., Żydak, M., Kwolek, B., Wąsowicz, P., Bukała, A., Swadźba, J., Sitkowski, P.: DiagSet: a dataset for prostate cancer histopathological image classification. Scientific Reports. 14, 1–14 (2024). https://doi.org/10.1038/s41598-024-52183-4.
12. Angel Latha Mary, S., Siva Subramanian, S., Priyanka, G., Vijayakumar, T., Alagumalai, S.: Revolutionizing prostate cancer diagnosis: Unleashing the potential of an optimized deep belief network for accurate Gleason grading in histological images. International Journal of Intelligent Networks. 5, 241–254 (2024). https://doi.org/10.1016/j.ijin.2024.05.004.
13. Santa-Rosario, J.C., Gustafson, E.A., Sanabria Bellassai, D.E., Gustafson, P.E., de Socarraz, M.: Validation and three years of clinical experience in using an artificial intelligence algorithm as a second read system for prostate cancer diagnosis—real-world experience. Journal of Pathology Informatics. 15, 100378 (2024). https://doi.org/10.1016/j.jpi.2024.100378.
14. Kondejkar, T., Al-Heejawi, S.M.A., Breggia, A., Ahmad, B., Christman, R., Ryan, S.T., Amal, S.: Multi-Scale Digital Pathology Patch-Level Prostate Cancer Grading Using Deep Learning: Use Case Evaluation of DiagSet Dataset. Bioengineering. 11, (2024). https://doi.org/10.3390/bioengineering11060624.
15. Dominguez-Morales, J.P., Duran-Lopez, L., Marini, N., Vicente-Diaz, S., Linares-Barranco, A., Atzori, M., Müller, H.: A systematic comparison of deep learning methods for Gleason grading and scoring. Medical Image Analysis. 95, 103191 (2024). https://doi.org/10.1016/j.media.2024.103191.
16. Butt, M.A., Kaleem, M.F., Bilal, M., Hanif, M.S.: Using multi-label ensemble CNN classifiers to mitigate labelling inconsistencies in patch-level Gleason grading. PLoS ONE. 19, 1–24 (2024). https://doi.org/10.1371/journal.pone.0304847.
17. Alici-Karaca, D., Akay, B.: An efficient deep learning model for prostate cancer diagnosis. IEEE Access. 12, 150776–150792 (2024). https://doi.org/10.1109/ACCESS.2024.3472209.
18. Patkar, S., Harmon, S., Sesterhenn, I., Lis, R., Merino, M., Young, D., Brown, G.T., Greenfield, K.M., McGeeney, J.D., Elsamanoudi, S., Tan, S.H., Schafer, C., Jiang, J., Petrovics, G., Dobi, A., Rentas, F.J., Pinto, P.A., Chesnut, G.T.,

Choyke, P., Turkbey, B., Moncur, J.T.: A selective CutMix approach improves generalizability of deep learning-based grading and risk assessment of prostate cancer. Journal of Pathology Informatics. 15, (2024). https://doi.org/10.1016/j.jpi.2024.100381.

19. Zhang, H., Patkar, S., Lis, R., Merino, M.J., Pinto, P.A., Choyke, P.L., Turkbey, B., Harmon, S.: Masked Image Modeling Meets Self-Distillation: A Transformer-Based Prostate Gland Segmentation Framework for Pathology Slides. Cancers. 16, 1–12 (2024). https://doi.org/10.3390/cancers16233897.
20. Ozbozduman, K., Loc, I., Durmaz, S., Atasoy, D., Kilic, M., Yildirim, H., Esen, T., Vural, M., Unlu, M.B.: Machine learning prediction of Gleason grade group upgrade between in-bore biopsy and radical prostatectomy pathology. Scientific Reports. 14, 1–11 (2024). https://doi.org/10.1038/s41598-024-56415-5.
21. Kong, F., Wang, X., Xiang, J., Yang, S., Wang, X., Yue, M., Zhang, J., Zhao, J., Han, X., Dong, Y., Zhu, B., Wang, F., Liu, Y.: Federated attention consistent learning models for prostate cancer diagnosis and Gleason grading. Computational and Structural Biotechnology Journal. 23, 1439–1449 (2024). https://doi.org/10.1016/j.csbj.2024.03.028.
22. Zhu, L., Pan, J., Mou, W., Deng, L., Zhu, Y., Wang, Y., Pareek, G., Hyams, E., Carneiro, B.A., Hadfield, M.J., El-Deiry, W.S., Yang, T., Tan, T., Tong, T., Ta, N., Zhu, Y., Gao, Y., Lai, Y., Cheng, L., Chen, R., Xue, W.: Harnessing artificial intelligence for prostate cancer management. Cell Reports Medicine. 5, (2024). https://doi.org/10.1016/j.xcrm.2024.101506.
23. Eminaga, O., Saad, F., Tian, Z., Wolffgang, U., Karakiewicz, P.I., Ouellet, V., Azzi, F., Spieker, T., Helmke, B.M., Graefen, M., Jiang, X., Xing, L., Witt, J.H., Trudel, D., Leyh-Bannurah, S.-R.: Artificial intelligence unravels interpretable malignancy grades of prostate cancer on histology images. npj Imaging. 2, 1–12 (2024). https://doi.org/10.1038/s44303-023-00005-z.
24. Khalid, U., Gurung, J., Doykov, M., Kostov, G., Hristov, B., Uchikov, P., Kraeva, M., Kraev, K., Doykov, D., Doykova, K., Valova, S., Chervenkov, L., Tilkiyan, E., Eneva, K.: Artificial Intelligence Algorithms and Their Current Role in the Identification and Comparison of Gleason Patterns in Prostate Cancer Histopathology: A Comprehensive Review. Diagnostics. 14, (2024). https://doi.org/10.3390/diagnostics14192127.
25. Agosti, V., Munari, E.: Histopathological evaluation and grading for prostate cancer: current issues and crucial aspects. Asian Journal of Andrology. 575–581 (2024). https://doi.org/10.4103/aja202440.
26. Schmidt, B., Soerensen, S.J.C., Bhambhvani, H.P., Fan, R.E., Bhattacharya, I., Choi, M.H., Kunder, C.A., Kao, C.S., Higgins, J., Rusu, M., ASonn, G.A.: External validation of an artificial intelligence model for Gleason grading of prostate cancer on prostatectomy specimens. BJU International. 133–139 (2024). https://doi.org/10.1111/bju.16464.
27. Marrón-Esquivel, J.M., Duran-Lopez, L., Linares-Barranco, A., Dominguez-Morales, J.P.: A comparative study of the inter-observer variability on Gleason grading against Deep Learning-based approaches for prostate cancer. Computers in Biology and Medicine. 159, 106856 (2023). https://doi.org/10.1016/j.compbiomed.2023.106856.
28. Nishio, M., Matsuo, H., Kurata, Y., Sugiyama, O., Fujimoto, K.: Label Distribution Learning for Automatic Cancer Grading of Histopathological Images of Prostate Cancer. Cancers. 15, 1–12 (2023). https://doi.org/10.3390/cancers15051535.
29. Zhuang, H., Chatterjee, A., Fan, X., Qi, S., Qian, W., He, D.: A radiomics based method for prediction of prostate cancer Gleason score using enlarged region of interest. BMC Medical Imaging. 23, 1–11 (2023). https://doi.org/10.1186/s12880-023-01167-3.
30. Fogarty, R., Goldgof, D., Hall, L., Lopez, A., Johnson, J., Gadara, M., Stoyanova, R., Punnen, S., Pollack, A., Pow-Sang, J., Balagurunathan, Y.: Classifying Malignancy in Prostate Glandular Structures from Biopsy Scans with Deep Learning. Cancers. 15, (2023). https://doi.org/10.3390/cancers15082335.
31. Kiełb, P., Kowalczyk, K., Gurwin, A., Nowak, Ł., Krajewski, W., Sosnowski, R., Szydełko, T., Małkiewicz, B.: Novel Histopathological Biomarkers in Prostate Cancer: Implications and Perspectives. Biomedicines. 11, 1–27 (2023). https://doi.org/10.3390/biomedicines11061552.
32. Bulten, W., Kartasalo, K., Chen, PH.C. et al. Artificial intelligence for diagnosis and Gleason grading of prostate cancer: the PANDA challenge. Nat Med (2022). https://doi.org/10.1038/s41591-021-01620-2.